Determination of Shape, Gravity, and Rotational State of Asteroid 433 Eros

ARTICLE *in* ICARUS · JANUARY 2002

Impact Factor: 3.04 · DOI: 10.1006/icar.2001.6753

Icarus **155**, 3–17 (2002)
doi:10.1006/icar.2001.6753, available online at http://www.idealibrary.com on IDEAL®

Determination of Shape, Gravity, and Rotational State of Asteroid 433 Eros

J. K. Miller, A. S. Konopliv, P. G. Antreasian, J. J. Bordi, S. Chesley, C. E. Helfrich, W. M. Owen, T. C. Wang, B. G. Williams, and D. K. Yeomans

Jet Propulsion Laboratory, California Institute of Technology, 4800 Oak Grove Drive, Pasadena, California 91109
E-mail: jkmiller@jpl.nasa.gov

and

D. J. Scheeres

Department of Aerospace Engineering, The University of Michigan, Ann Arbor, Michigan 48109

Received December 18, 2000; revised August 22, 2001

Prior to the Near Earth Asteroid Rendezvous (NEAR) mission, little was known about Eros except for its orbit, spin rate, and pole orientation, which could be determined from ground-based telescope observations. Radar bounce data provided a rough estimate of the shape of Eros. On December 23, 1998, after an engine misfire, the NEAR-Shoemaker spacecraft flew by Eros on a high-velocity trajectory that provided a brief glimpse of Eros and allowed for an estimate of the asteroid's pole, prime meridian, and mass. This new information, when combined with the ground-based observations, provided good *a priori* estimates for processing data in the orbit phase.

After a one-year delay, NEAR orbit operations began when the spacecraft was successfully inserted into a 320 × 360 km orbit about Eros on February 14, 2000. Since that time, the NEAR spacecraft was in many different types of orbits where radiometric tracking data, optical images, and NEAR laser rangefinder (NLR) data allowed a determination of the shape, gravity, and rotational state of Eros. The NLR data, collected predominantly from the 50-km orbit, together with landmark tracking from the optical data, have been processed to determine a 24th degree and order shape model. Radiometric tracking data and optical landmark data were used in a separate orbit determination process. As part of this latter process, the spherical harmonic gravity field of Eros was primarily determined from the 10 days in the 35-km orbit. Estimates for the gravity field of Eros were made as high as degree and order 15, but the coefficients are determined relative to their uncertainty only up to degree and order 10. The differences between the measured gravity field and one determined from a constant density shape model are detected relative to their uncertainty only to degree and order 6. The offset between the center of figure and the center of mass is only about 30 m, indicating that Eros has a very uniform density (1% variation) on a large scale (35 km). Variations to degree and order 6 (about 6 km) may be partly explained by the existence of a 100-m, regolith or by small internal density variations. The best estimates for the J2000 right ascension and declination of the pole of Eros are $\alpha = 11.3692 \pm 0.003^\circ$ and $\delta = 17.2273 \pm 0.006^\circ$. The rotation rate of Eros is $1639.38922 \pm 0.00015^\circ$/day, which gives a rotation period of 5.27025547 h. No wobble greater than 0.02° has been detected. Solar gravity gradient torques would introduce a wobble of at most 0.001°.

Key Words: **Eros; asteroid; shape; gravity harmonics; rotation state.**

INTRODUCTION

The original plan for Eros orbit insertion (Farquhar 1995) called for a series of rendezvous burns beginning on December 20, 1998, that would insert the NEAR spacecraft into Eros obrit in January 1999. As a result of an unplanned termination of the first rendezvous burn (Dunham *et al*. 1999), NEAR continued on its high-velocity approach trajectory and passed within 3900 km of Eros on December 23, 1998. At this time, it was not possible to place the NEAR spacecraft in orbit about Eros. Instead, a modified rendezvous burn was executed on January 3, 1999, which resulted in the spacecraft being placed on a trajectory that slowly returned to Eros with a subsequent delay of the Eros orbit insertion maneuver until February 2000. The flyby of Eros provided a brief glimpse and allowed for a crude estimate of the pole and prime meridian with an error of 2° and a 10% mass solution (Miller *et al*. 1999, Yeomans *et al*. 1999). Orbital operations commenced on February 14, 2000, with an orbit insertion burn that placed the spacecraft into a nearly circular 350-km orbit. A series of propulsive burns lowered the spacecraft orbit to a 50-km and then a 35-km circular orbit where the data acquired allowed precise estimates of Eros' physical parameters. Table I lists the orbit phases for the NEAR mission included in this study from the beginning orbit phase on February 14, 2000, to the close flyby within 5 km of the surface of Eros on October 25, 2000.

0019-1035/02 $35.00

TABLE I
Eros Orbit Segments

Segment	Start date, time (UTC)	Length (days)	Orbit (km × km)	Period (days)	Inclination (deg.) ATE[a]	Inclination (deg.) SPOS[b]
1	2/14/00 15:33	10.1	366 × 318	21.8	35	176
2	2/24/00 17:00	8.1	365 × 204	16.5	33	172
3	3/3/00 18:00	29.3	205 × 203	10.0	37	171
4	4/2/00 02:03	9.8	210 × 100	6.6	55	178
5	4/11/00 21:20	10.8	101 × 99	3.4	59	177
6	4/22/00 17:50	8.0	100 × 50	2.2	64	179
7	4/30/00 16:15	68.1	51 × 49	1.2	90	160
8	7/7/00 18:00	6.3	50 × 35	1.0	90	165
9	7/14/00 03:00	10.6	37 × 35	0.7	90	163
10	7/24/00 17:00	7.1	50 × 37	1.0	90	161
11	7/31/00 20:00	8.2	51 × 49	1.2	90	159
12	8/8/00 23:25	18.0	52 × 50	1.2	105	178
13	8/26/00 23:25	10.0	102 × 49	2.3	112	179
14	9/5/00 23:00	37.3	102 × 100	3.5	115	150
15	10/13/00 05:45	7.6	100 × 50	2.2	130	179
16	10/20/00 21:40	5.0	52 × 50	1.2	133	178
17	10/25/00 22:10	0.8	50 × 20	0.7	133	168

[a] ATE, asteroid true equator.
[b] SPOS, Sun plane of sky.

Estimates of the initial attitude and spin rate of Eros, as well as of reference landmark locations used for optical navigation, were obtained from images of the asteroid. In the planned navigation strategy, these initial estimates were used as *a priori* values for a more precise refinement of these parameters by an orbit determination technique which processes optical measurements combined with Doppler and range tracking. Although laser altimetry could be included in the orbit determination process, these data were processed separately using the orbits determined from the optical and radiometric data. The orbit determination software estimates the spacecraft state, asteroid attitude, asteroid ephemeris, solar pressure, landmark locations, measurement biases, spacecraft maneuvers, and Eros' physical parameters including its mass, moments of inertia, and gravity harmonics.

In addition to allowing accurately determined orbits about Eros, the gravity harmonics place constraints on the internal structure of Eros. The shape model was obtained by processing optical landmark and laser altimetry data. This shape model was then integrated over the entire volume, assuming constant density, to produce a predicted gravity field. A comparison of the true gravity field with this predicted gravity field from the shape model then provides insight into Eros' internal structure. The location of the center of mass derived from the first-degree harmonic coefficients directly indicates the overall mass distribution. The second-degree harmonic coefficients provide insight into the orientation of Eros' principal axes. Higher degree harmonics may be compared with surface features to gain additional insight into mass distribution. Preliminary and more recent results for the gravity and shape models have been presented by Miller *et al*. (2000), Yeomans *et al*. (2000), Veverka *et al*. (2000), Zuber *et al*. (2000), and Thomas *et al*. (2002).

ORBIT DETERMINATION STRATEGY

Several strategies have been used to determine the NEAR orbits and the physical parameters of Eros. The first technique uses PCODP software to process spacecraft Doppler and range data along with optical landmark observations over data arcs of 30 days or less. The second technique uses an independent software set, the Orbit Determination Program (ODP), to process spacecraft Doppler and range data arcs that can include the entire orbital phase of the NEAR spacecraft. PCODP was developed specifically for a mission in orbit about an asteroid or comet (Miller *et al*. 1990). For this approach, the data types used for determining NEAR's orbit are radiometric X-band (8.4-GHz downlink) Doppler and range and optical imaging of landmarks. A square-root information filter is used to process the data and this sequential filter is designed to handle up to 800 estimated parameters including 18 stochastic parameters. This parameter set includes initial spacecraft state, propulsive maneuvers, solar pressure parameters, stochastic accelerations, Eros' ephemeris, Eros' attitude and rotation state, and physical parameters that describe the size, shape, and gravity of Eros. Eros' physical parameters include gravitational harmonics to degree and order 12, inertia tensor elements, and the location of over 100 landmarks. The solution for nongravitational accelerations presents a particular challenge to the orbit determination filter. These accelerations include attitude control gas leaks and solar pressure. The solar pressure is modeled as a collection of reflecting surfaces with 12 separate parameters. Solar pressure mismodeling and any residual accelerations associated with outgassing from the spacecraft are lumped together and treated both as a constant acceleration and as stochastic

accelerations. The stochastic accelerations are modeled as three orthogonal independent exponentially correlated process noise components with an amplitude of 1×10^{-12} km/s^2 and a correlation time of 1 day. The total number of estimated parameters for this particular study was 608.

The differences in the moments of inertia may be determined from the gravity harmonic coefficients, but a particular moment of inertia about any axis cannot be determined from this difference alone (Miller *et al.* 1990). In the PCODP, the joint solution for both the gravity and rotational motion of Eros permits a determination of the principal moments of inertia provided the angular acceleration (or wobble about the principal axes) can be detected by the orbit determination filter.

The solution strategy involved processing several days of data at a time to converge slowly on the orbit solution. First, about two days of data are processed and the solution is fed back to the filter and the data are processed again. This process is repeated until convergence is achieved. At this point several more days of data are introduced to the filter and processed iteratively until another solution is obtained. Additional data are introduced in batches of several days until all the data are processed. Otherwise, processing longer batches of data, especially at the beginning of the mission, resulted in divergence. Once the filtering is complete, spacecraft trajectory, Eros ephemeris, and Eros attitude files are produced containing Chebyshev polynomials as a function of time. Gravity harmonic, landmark location, maneuver parameter, and shape harmonic coefficient files are also produced. With the PCODP approach, solutions for the physical parameters of Eros are limited to one data arc of length of about 30 days. While the longer data arc solutions using the ODP software provide the best gravity results, the PCODP technique, because of the inclusion of optical data, provided the best orbits for processing the NEAR laser rangefinder (NLR) data.

Optical tracking of landmarks in the imaging data taken by NEAR's multispectral imager (MSI; Hawkins *et al.* 1997) is a powerful data type for determining NEAR's trajectory and the rotation of Eros. Tracking individual landmarks, which are small craters, enables orbit determination accuracies on the order of the camera resolution or several meters. This exceeds the accuracy that can be obtained from radiometric data alone, from fitting limb data or from any measurement scheme that depends on the development of a precise shape model. We need only develop a data base of landmarks and identify the landmarks on more than one image to obtain useful information about the spacecraft orbit or Eros' rotation. The procedure of identifying and cataloging landmarks is aided by referring the landmarks to a model of the topographic surface or shape model. The actual identification of individual landmarks depends upon observing them in an image having many landmarks of various sizes to provide a context.

In addition to the one data arc (July 3 to August 7) used to determine the gravity field and rotation of Eros, three other data arcs were used to process the NLR data (April 30 to June 1, June 1 to July 3, and August 7 to September 12). For all the data arcs, the attitude of Eros is fixed to the solution obtained from the gravity solution data arc. This is done to maintain consistency when comparing the estimated gravity solution with the shape model gravity solution. Once a good solution was obtained for both the spacecraft trajectory and Eros' attitude as a function of time, some additional processing was required to transform the results to a more usable format and to solve for the shape. The solution for the shape of Eros is obtained by processing NLR data in a separate program that reads the spacecraft ephemeris and Eros attitude files.

The second approach uses the ODP (Moyer 1971) to process the Doppler and range data. Although the ODP has the capability of integrating the attitude of Eros similar to the PCODP, this option is not used. The attitude of Eros is assumed to be near principal axis rotation and the attitude of Eros is given by the right ascension (α) and declination (δ) of the pole and the prime meridian at the J2000 epoch together with a fixed rotation rate. The major difference with this approach is that it does not include the optical data as given by the landmark observations. However, it does include all the radiometric data processed to date (as listed in Table I) by using a multiple arc technique similar to that of previous planetary gravity efforts (e.g., Konopliv *et al.* 1999). The two approaches allow us to independently confirm solutions for the gravity field (including GM) and the rotation of Eros. It also reveals the differences resulting from independent stochastic models and gives us information on the strengths of the optical data. This two-approach technique provides insight into how the optical data improve the Eros pole solution, the orbit of the NEAR spacecraft, and the gravity field.

The ODP also uses a least-squares square-root information filter to solve for the spacecraft state in the coordinate system defined by the Earth's mean equator at the J2000 epoch. The radiometric data are broken into independent arcs that are at most one-month long but do not include any major orbit maneuvers (i.e., each data arc remains in just one section of Table I). The arcs are also at least one-week long except that the close approach arc on October 25 is 19-h long. The estimated parameters are arc-dependent variables (spacecraft state, etc.) that are determined separately for each data arc and global variables (harmonic coefficients, etc.) that are common to all data arcs. The global parameters are determined by merging only the global parameter portion of the square-root information arrays from all the arcs, a technique that is equivalent to solving for the global parameters plus arc-dependent parameters of all arcs. This technique (Kaula 1966, Ellis 1980) was first used to analyze Earth orbiter data.

Initially, each data arc is converged by estimating only the local variables while holding the global variables fixed to the nominal values. For each arc, the local variables estimated are similar to those in the PCODP approach. The local variables are limited to the spacecraft position and velocity, solar pressure, momentum wheel desaturation velocity increments, and range biases for each station pass. With the ODP method, the solar pressure is treated as stochastic and no additional stochastic acceleration model is used. The model is a simple

bus model with the primary acceleration in the Sun–spacecraft direction but with orthogonal accelerations (norminally zero) in the ecliptic plane and normal to the ecliptic. The *a priori* uncertainty on the solar pressure model for all three directions is about 5% of the solar pressure force in the Sun–spacecraft direction, and the time constant is taken to be 12 h. The global parameters estimated from all the NEAR radiometric data between February 14 and October 26, 2000, are the ephemeris of Eros, the right ascension and declination of the pole, the rotation rate, the GM, and the gravity field to degree and order 15.

Although Eros is a very irregular body, the gravitational potential for both methods can be modeled with a spherical harmonic expansion with normalized coefficients ($\bar{C}_{nm}$, $\bar{S}_{nm}$) given by

$$U = \frac{GM}{r}\sum_{n=0}^{\infty}\sum_{m=0}^{n}\left(\frac{r_0}{r}\right)^n \bar{P}_{nm}(\sin\phi) \times [\bar{C}_{nm}\cos(m\lambda) + \bar{S}_{nm}\sin(m\lambda)],$$

where n is the degree and m is the order, $\bar{P}_{nm}$ are the fully normalized Legendre polynomials and associated functions, r_0 is the reference radius of Eros (16.0 km for our models), ϕ is the latitude, and λ is the longitude. The normalized coefficients are related to the unnormalized ones by (Kaula 1966)

$$(\bar{C}_{nm}; \bar{S}_{nm}) = \left[\frac{(n+m)!}{(2-\delta_{0m})(2n+1)(n-m)!}\right]^{\frac{1}{2}}(C_{nm}; S_{nm}),$$

where δ_{0m} is the Kronecker delta function. The harmonic coefficients of degree one are fixed to zero since the origin of the coordinate system is chosen to be the center of mass of the body. This expansion converges outside the smallest sphere enclosing Eros (Heiskanen and Moritz 1967). All the NEAR data employed are outside this sphere and so using spherical harmonics is the simplest way to compare the gravity and shape models. All gravity and shape results are mapped onto a sphere of radius 16 km. For mapping the gravity field to the surface of Eros, one must use alternative methods such as direct integration over the volume of Eros defined by the shape model, a polyhedra representation of the same shape model (Werner and Scheeres 1997), or ellipsoidal harmonics (Garmier and Barriot 2000).

THE EROS *A PRIORI* PHYSICAL MODEL

Determination of the spacecraft orbit about Eros is intimately associated with the development of an accurate physical model of Eros. Eros is the principal source of perturbations on the spacecraft's trajectory and therefore the principal source of data for determining the orbit. The model of Eros used for orbit determination is similar to the model used for science investigation. The major difference is in emphasis of detail.

During a particularly close Earth approach (0.15 AU) in January 1975, there was a coordinated ground-based observation campaign to characterize the physical nature of Eros. Photometric, spectroscopic, and radar measurements provided a diverse data set that allowed the asteroid's size, shape, and spectral class to be determined (see Veverka *et al*. 2000, Yeomans 1995). Eros is an S-class asteroid with a geometric albedo of about 0.27. The absolute magnitude of Eros (at 0° phase angle and 1 AU from both the Sun and Earth) is 11.16. From the lightcurve, which reaches 1.47 magnitudes in amplitude, the rotation period and pole direction were determined. During the December 1998 flyby, crude estimates of Eros' mass and pole location were obtained (Miller *et al*. 1999, Yeomans *et al*. 1999, Veverka *et al*. 1999). The pole location confirmed ground-based measurements to an accuracy of about 2°. Observation of the lit portions of Eros by the MSI permitted a rough shape determination. The gravity harmonic coefficients were computed from this shape determination by numercial integration assuming constant density. Lightcurve data obtained during the flyby yielded a precise rotation rate for Eros and enabled location of the prime meridian with respect to a large crater discernible in the images. This information was used as *a priori* data for the orbit phase solution presented here.

ORBIT DETERMINATION SOLUTION

In addition to the models describing the estimated parameters, calibrations obtained from other models are applied to the Doppler, range, and optical data. The calibration data included seasonal and daily troposphere and ionosphere models based upon on-site GPS and weather measurements and a solar plasma model. DSN station locations are modeled to about 4-cm accuracy with Earth precession, nutation, polar motion, ocean tidal loading, solid Earth tide, and tectonic plate motion. A landmark file consisting of *a priori* landmark locations and unique identification numbers was assembled along with a picture sequence file that contained camera pointing and image coordinates for each landmark that was identified. Additional models that were needed for estimation include the spacecraft clock model, solar pressure model, and propulsive maneuvers. Initial state vectors for the equations describing the motion of the spacecraft, planets, and Eros are also required.

The PCODP gravity and pole solution data arc, which included Doppler, range, and optical imaging of landmarks, extended from July 3, 2000, through August 7, 2000. Nearly continuous Doppler data were processed and the postfit residuals for this solution are shown in Fig. 1. The ordinate is the measurement residual in hertz. A spacecraft radial velocity component of 1 mm/s measured along the line of sight from a particular DSN tracking station corresponds to approximately 0.054 Hz of Doppler shift over the count time interval, which is typically 60 s. The Doppler signature shown on Fig. 1 reveals noise with an amplitude of 0.002 Hz (0.03 mm/s) rms.

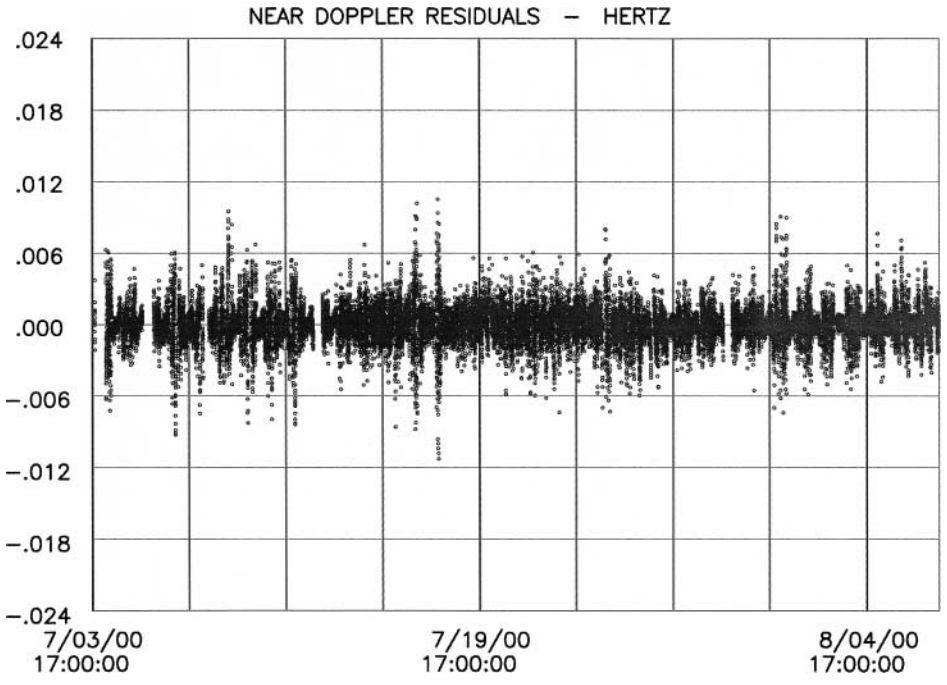

FIG. 1. NEAR spacecraft Doppler residuals from the PCODP solution spanning the 35-km orbit phase. Shown are individual DSN station tracking data passes from July 3 to August 7, 2000.

Optical data residuals are shown in Fig. 2. The ordinate of this figure is the measurement error in pixel (x) or line (y) direction in an image. One line subtends 165 microradians and one pixel subtends 95 microradians. In a 50-km orbit, the line and pixel measurement errors translate to 5.8 m and 3.3 m respectively when observing landmarks on the ends of Eros at a range of about 35 km. The rms of the measurement error is about 2 lines and pixels and permits submeter accuracy when the more than

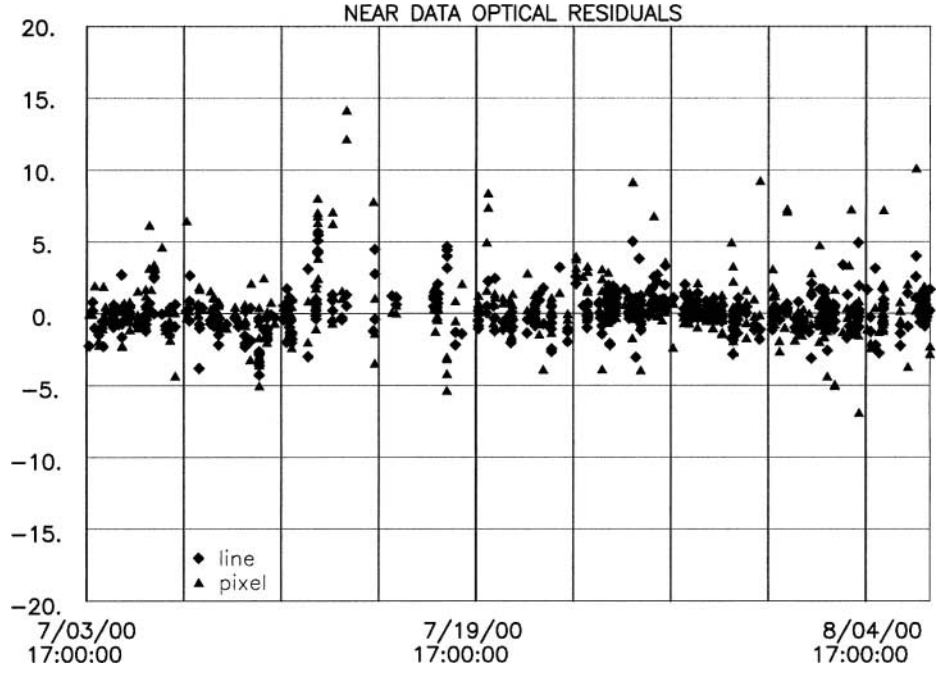

FIG. 2. NEAR spacecraft optical data residuals from the PCODP solution spanning the 35-km orbit phase. During the time interval from July 3 to August 7, 2000, the spacecraft range to Eros varied from 19 to 42 km. This corresponds to a position measurement error on the surface of Eros that varies from 1.8 to 4.0 m in pixels and 3.1 to 6.9 m in lines.

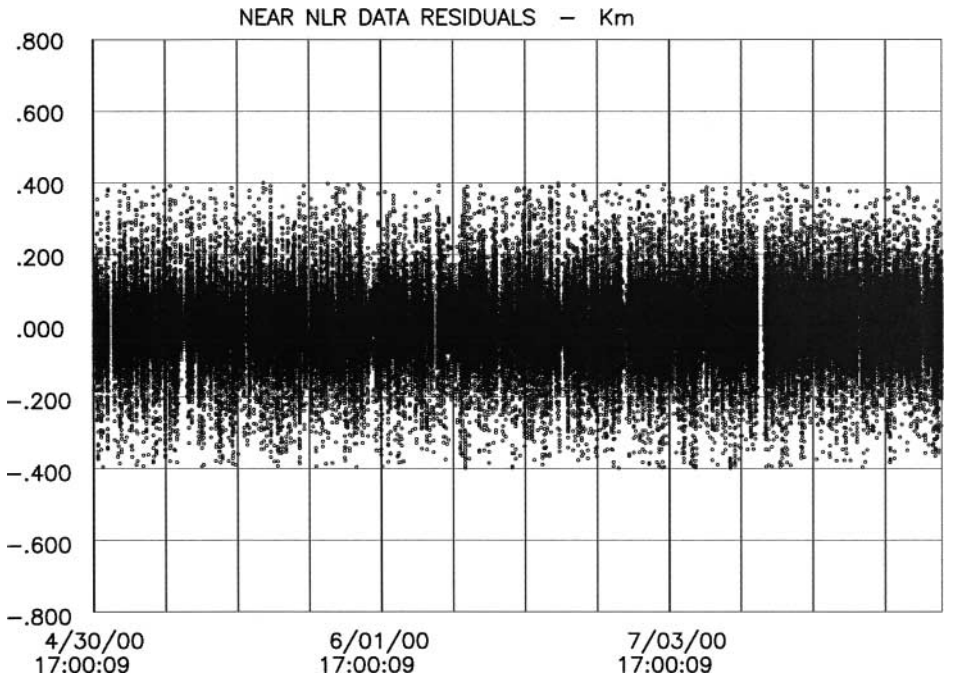

FIG. 3. NEAR spacecraft NLR residuals. The rms error is about 100 m after data points with an error greater than 400 m are rejected.

3000 optical observations are processed by the orbit determination filter. The PCODP orbit solution from the 35-km data arc with the radiometric and optical data was compared to the ODP radiometric-only solution and the rms differences were less than 10 m in all three directions (radial, downtrack, and crosstrack), indicating the high accuracy of the orbits. High-precision orbits are obtained by processing optical data since individual landmarks may be located with an accuracy of a few meters with respect to the center of mass. With the optical data giving highly accurate orbits, the range data tie down the Eros ephemeris.

Including the NLR data in the orbit determination solution does not improve the spacecraft orbit. The shape model has errors on the order of a hundred meters, which is far greater than the orbit error. However, the NLR data were useful for determining a shape model that is accurate to about 100 m. This was accomplished by processing a high-precision spacecraft ephemeris file and Eros attitude file, obtained from the orbit determination solution, in a separate program that solves only for the shape model harmonic coefficients and NLR bias parameters. The postfit residuals are shown in Fig. 3. The rms error is 109 m and measurement errors greater than 400 m were rejected by the filter. The large rms error of the NLR measurement belies the accuracy of the NLR since this residual error is dominated by modeling errors in determining the shape. The instrument error is only a few meters. Since the modeling error is unbiased, a considerable reduction in the determination of the mean radius of Eros may be expected when the 263,490 NLR observations are processed. Eros' volume may be estimated to an accuracy of 1% using this solution strategy.

RESULTS FOR EROS

The solution for Eros' physical parameters is summarized in Table II. The mass and volume combine to give a bulk density of 2.67 g/cm^3 with an accuracy of 1%. The mass, volume, and bulk density values reported here confirm the preliminary estimates given by Miller *et al*. (2000) and Yeomans *et al*. (2000).

Table II shows that the optical-based solution (from the PCODP) provides the best estimate of the pole location by about a factor of 3, although the radiometric solution (ODP) is consistent within its uncertainty. The errors for the pole and *GM* are formal statistical errors from the solution covariance but scaled higher by a factor of 3 to give a more realistic error. The *GM* solution based upon the radiometric data only is very sensitive to the initial pole value and to whether it is estimated. The *GM* solution with the optical data is 10 times more accurate than the radiometric-only solution. However, when the pole is fixed to the optically determined values, the radiometric *GM* solution agrees well with the optical solution and the uncertainty decreases. The radiometric rotation rate solution is nearly three times better than the optical solution. This is most likely due to the radiometric data set including data from the entire NEAR mission while the optical solution is limited to about 30 days of data.

Shape Model

The Eros shape model obtained from the NLR data is in the form of harmonic coefficients through degree and order 24. One may use the harmonic expansion to compute the radius of Eros as a function of latitude and longitude. The resulting topographic

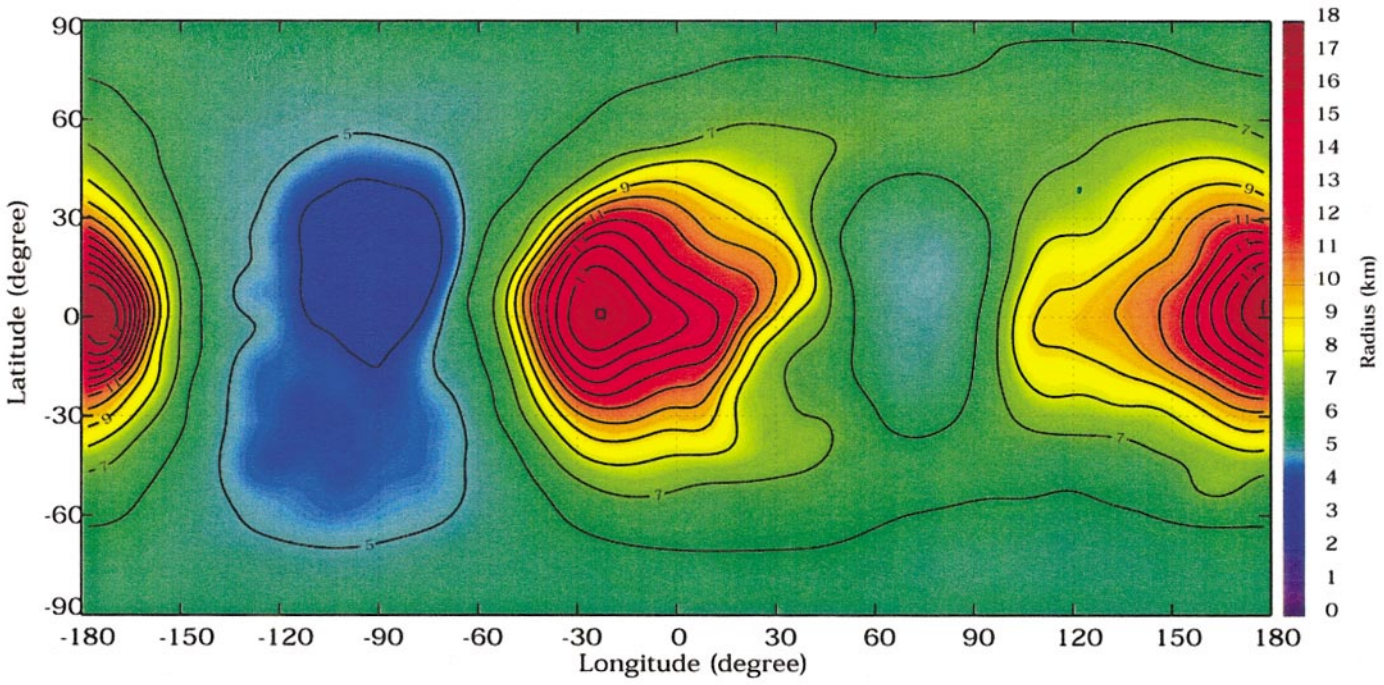

FIG. 4. The Eros shape model from the spherical harmonic solution to degree and order 24. Displayed are radial distances from the center of mass. The minimum distance is 3.19 km and the maximum is 17.67 km.

TABLE II
Solution for Eros Physical Parameters

Parameters	Values
Size and density	
Volume	2503 ± 25 km^3
Bulk density	2.67 ± 0.03 g/cm^3
X_{cg} of figure	-9.7 m
Y_{cg} of figure	2.4 m
Z_{cg} of figure	32.6 m
Mass properties	
Mass	$(6.6904 \pm 0.003) \times 10^{15}$ kg
GM (optical radiometric)	$(4.4631 \pm 0.0003) \times 10^{-4}$ km^3/s^2
GM (radiometric)	$(4.4584 \pm 0.0030) \times 10^{-4}$ km^3/s^2
GM (radiometric and optical pole)	$(4.4621 \pm 0.0015) \times 10^{-4}$ km^3/s^2
I_{xx} (normalized)	17.09 km^2
I_{yy} (normalized)	71.79 km^2
I_{zz} (normalized)	74.49 km^2
X principal axis	9.29 deg East (definition)
Pole (optical)	
Right ascension	11.369 ± 0.003 deg
Declination	17.227 ± 0.006 deg
Rotation rate	1639.38885 ± 0.0005 deg/day
Prime meridian	326.06 deg (at epoch and equinox J2000)
Pole (radiometric)	
Right ascension	11.363 ± 0.01 deg
Declination	17.230 ± 0.02 deg
Rotation rate	1639.38922 ± 0.0002 deg/day

map, shown in Fig. 4, reveals two mountainous looking features about the size of Mount Everest. This is an illusion since these features are simply the elongated ends of Eros. The contour lines shown are accurate to about 100 m, and this can be verified by comparing the shape of Eros projected into two dimensions to actual images of Eros taken by the MSI. Where the curvature is great, the shape model error is as high as 200 m.

The accuracy of the shape model may also be confirmed by computing the radius vectors for reference landmarks, the locations of which have been determined to about 5 m. The locations of about 43 landmarks were confirmed to be on the shape model surface with an rms error of about 50 m. A few of the landmarks were above or below the shape model surface by as much as 200 m in the regions of Eros where the nadir-pointed NLR intersected the surface at a high incidence angle.

Even though the local variation in the shape model error suggests an accuracy of about 100 m, the error in determining the average radius integrated over the entire surface may be much smaller. The trajectory error and instrument measurement error combined are about 10 m. Since the shape model error associated with the harmonic coefficients is unbiased, the error in determining the average radius, which is directly related to the volume determination, may be reduced considerably by taking many measurements and statistically averaging. This averaging, which is implicity performed by the orbit determination filter, is effective when a large number of measurements are processed, since the error in the average radius is reduced by the square root of the number of measurements. For 263, 490 NLR

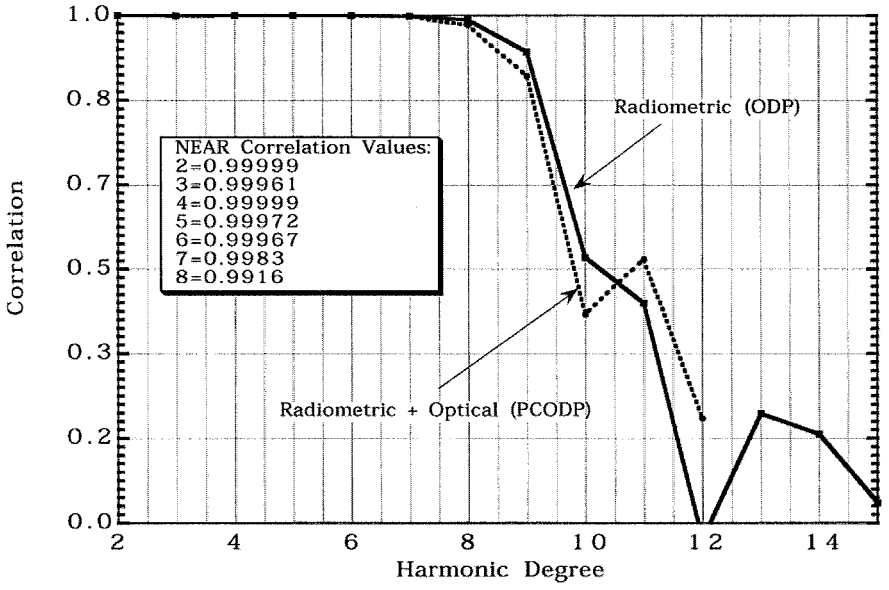

FIG. 5. The correlation of the estimated Eros gravity solutions with the gravity solution integrated from the shape model assuming constant density.

measurements, the modeling error may be reduced by a factor of about 500, which is well below the level where systematic errors dominate. Thus the volume of Eros and the low-order shape harmonic coefficients may be determined to an accuracy of 1% provided the surface is sampled randomly and systematic errors associated with the trajectory and instrument biases are about 10 m. The NLR data acquisition strategy for NEAR resulted in fairly uniform coverage of Eros, owing to the circular 50-km polar orbit and the relatively rapid rotation of Eros. The random character of the sampling is at very small scales. Statistically, NLR samples that measure the surface at the top of boulders are compensated by samples that fall in craters. This mathematical

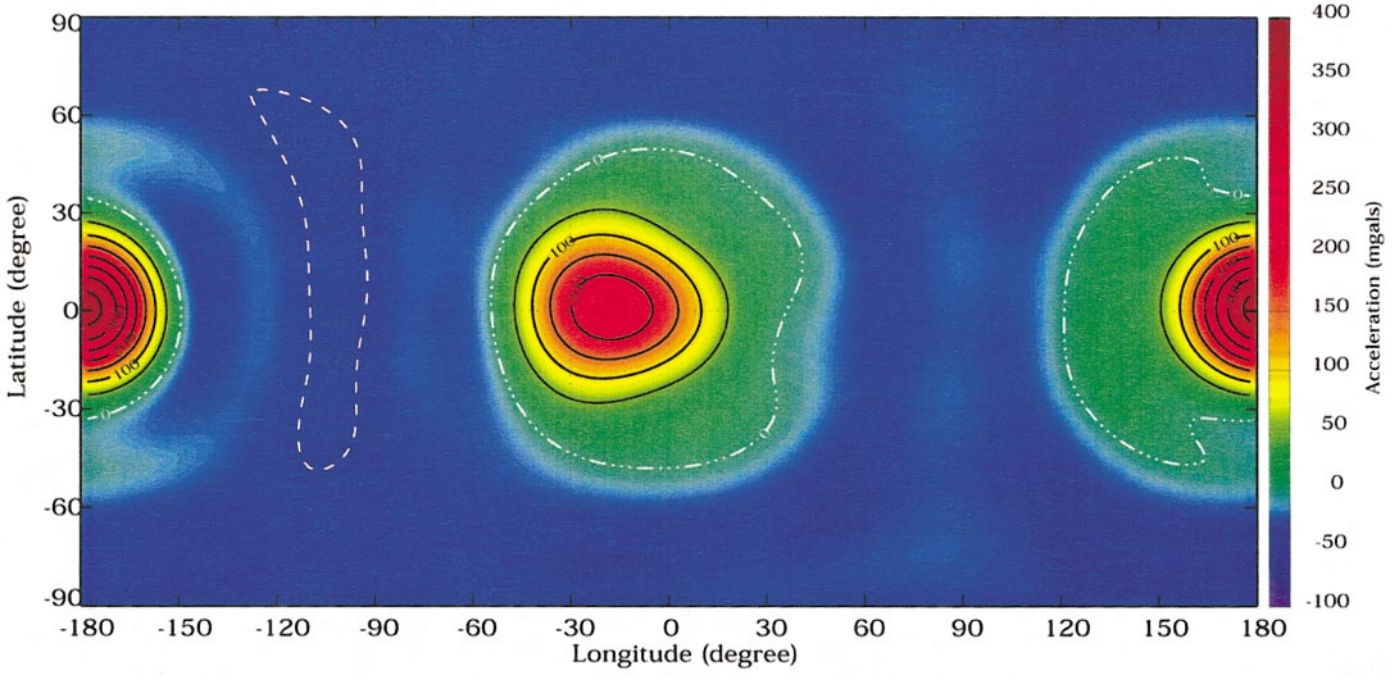

FIG. 6. The radial acceleration of the Eros gravity field (radiometric solution) on a sphere of 16 km radius for coefficients through degree 8. The contours have intervals of 20 mgal (1 mgal $= 10^{-8}$ km/s^2). Not included in the acceleration is the acceleration a particle on the sphere would feel due to rotation.

property of laser altimetry gives this method a distinct advantage over optical imaging, where shadows tend to obscure the surface at small scales.

Gravity Harmonics

Determination of the gravity harmonic coefficients of Eros is a direct result of the spacecraft orbit determination process necessary to navigate the spacecraft. The harmonic coefficients are estimated by observing the acceleration of the spacecraft in orbit. As the spacecraft is maneuvered closer to Eros, the degree of the harmonic expansion must be increased to provide the required accuracy for orbit prediction. This results in a determination of Eros' gravity field to fairly high precision. At degree 10, the uncertainty or noise in the gravity field is roughly equal to the signal as given by the rms of the coefficients. The rms differences between the coefficients of the two independent solutions (PCODP with optical and radiometric data and ODP with radiometric data only) are small. However, the differences between the two techniques at low degree are 2–3 times the formal uncertainty of the radiometric-only solution and this is partly the reason we choose to scale the formal errors by 3 for the gravity field and the results in Tables II and III. The small differences also show that the gravity field solution is dominated by the data in the 35-km orbit and the other orbits contribute very little to the solution. In contrast to the pole solution, the optical data do not significantly contribute to the gravity solution.

TABLE III
Gravity Harmonic Coefficients

Coefficient ($R_0 = 16.0$ km)	Solution: Spacecraft dynamics	Solution: Shape model integration
C_{10}	0	0.001175
C_{11}	0	−0.000348
S_{11}	0	0.000088
C_{20}	−0.052478 (.000051)	−0.052851
C_{21}	0	0.000102
S_{21}	0	0.000012
C_{22}	0.082538 (.000061)	0.083203
S_{22}	−0.027745 (.000035)	−0.028033
C_{30}	−0.001400 (.000030)	−0.001747
C_{31}	0.004055 (.000006)	0.004083
S_{31}	0.003379 (.000006)	0.003404
C_{32}	0.001792 (.000016)	0.002129
S_{32}	−0.000686 (.000016)	−0.000836
C_{33}	−0.010337 (.000027)	−0.010456
S_{33}	−0.012134 (.000027)	−0.012247
C_{40}	0.012900 (.000070)	0.013077
C_{41}	−0.000106 (.000014)	−0.000145
S_{41}	0.000136 (.000015)	0.000165
C_{42}	−0.017495 (.000035)	−0.017656
S_{42}	0.004542 (.000030)	0.004589
C_{43}	−0.000319 (.000044)	−0.000312
S_{43}	−0.000141 (.000044)	−0.000195
C_{44}	0.017587 (.000062)	0.017729
S_{44}	−0.008939 (.000061)	−0.009048

An *a priori* gravity model can be developed by integrating the potential function over the shape model determined by NLR or MSI observations assuming constant density. The results are shown in Table III for comparison. The close agreement of the gravity coefficients obtained from spacecraft dynamics and those obtained from the NLR-derived shape model provides a high degree of confidence in the results when used for NEAR spacecraft navigation. Since the shape-derived gravity coefficients assumed a constant density, the closeness of the agreement for the two sets of coefficient values (Table III) indicates that the material within the interior of Eros is nearly of uniform density.

Of particular interest are the first degree and order terms of the harmonic expansions (C_{11}, S_{11}, C_{10}). For the spacecraft orbit solution, these terms were explicitly set to zero, forcing the center of the coordinate system to coincide with the center of mass of Eros. Thus, the values of these coefficients from the shape model provide a direct measure of the offset of the center of figure from Eros' center of mass. The vector from the origin to the center of mass may be determined by multiplying the first degree and order coefficients by the reference radius (16 km). For normalized gravity coefficients, an additional factor of $\sqrt{3}$ is required. Applying these factors to the coefficients shown in Table III reveals that the center-of-figure offset vector for Eros, obtained independently from NLR measurements, is (−9.7, 2.4, 32.6) m, as shown in Table II. This result indicates that the bulk density of the octants of Eros, defined arbitrarily by the planes of the reference coordinate axes, agree within 1%. This is another strong indication of the uniformity of Eros' internal structure.

Yet another indication of the uniformity of Eros' density is the correlation between the gravity harmonic coefficients obtained from spacecraft dynamics with those obtained from integration of the shape model. This correlation is computed for coefficients of a particular degree by taking the dot product of the coefficients and dividing by the respective norms. The results are shown in Fig. 5 for the two independent gravity solutions. The high degree of correlation for the lower degree coefficients for Eros is a strong indication of uniform density even though some of this correlation is inherent in the shape. The correlation is about 50% at degree 10 where the signal is equal to the noise.

The gravity field of Eros as a function of latitude and longitude is shown on Fig. 6 for harmonics up to degree 8. The gravity field is displayed in milligals (1 gal = 1 cm/s^2) on a sphere with a radius of 16 km. The central body (GM) term of the harmonic expansion is not included in computing the acceleration and this accounts for the negative values. Comparison of the gravity field map with the topographic map shown in Fig. 4 does not reveal a high degree of correlation. The ends of Eros stand out, but surface features on a smaller scale are not seen as would be

the case for the Moon or terrestrial planets. This is because the surfaces of constant gravity potential do not conform well to the shape of Eros and, when displayed on a sphere, the ends of Eros are given more weight than the central part. The advantage, however, for displaying the gravity field on a sphere is that the formal gravity uncertainty is very nearly uniform and is about 0.3 mgal for coefficients to degree 6 and 2.0 mgal to degree 8. Instead of using Fig. 4, we can obtain a more meaningful result by comparing the Eros gravity map with the gravity map obtained from the Eros shape model assuming constant density. Since the gravity map from Eros' shape would look very much like the actual Eros gravity map, the difference between the two maps is plotted as a function of latitude and longitude. This difference map (estimated gravity minus gravity from shape integration) is known as a Bouguer map and is shown in Fig. 7 for coefficients through degree 6. Differences in the gravity field, shown in Fig. 7, reveal peaks and valleys uniformly distributed over Eros with maxima and minima of 3–4 mgal. The Bouguer variations are about 10 times the formal uncertainty derived from the gravity covariance and these differences are about 1–2% of the maximum gravity amplitude. These differences, most likely, may be attributed to variations of mass, although for degree less than 6, the largest error contributions are from the shape model.

Given the Bouguer map, there is no unique solution for the mass distribution of Eros. Possible explanations for the observed mass deficiency at the ends of Eros include a less dense regolith covering on the order of 100 m distributed perhaps uniformly over the surface of Eros or a more dense concentration of material near the center of Eros. At degree 6, a 100-m uniform covering with a density contrast of 0.6 gm/cm^3 produces a signature of -1.0 and -0.4 mgal at the asteroid ends. The observed signature therefore requires a higher density contrast, thicker regolith, or a variable thickness regolith that may be correlated with greater thicknesses for the highest potential areas. The Bouguer map also displays a shift of the negative anomaly to the northern hemisphere, indicating less dense material there. This may be related to higher potential areas also being shifted to the north where less dense regolith may accumulate. Figure 8 shows the gravitational potential on the surface of Eros computed from a polyhedron gravity model (Werner and Scheeres 1997) corrected for Eros' rotation. Regions of high gravitational potential correspond to low regions on the surface of Eros where material may be expected to accumulate. An alternative explanation for the observed gravity anomaly is to attribute the distribution of mass to an increase in the density of the central core of Eros. An increase in density of 5% for the central part of Eros, in the form of a sphere with 20% of the volume of Eros, results in a -3.0 mgal signature in the Bouguer map and very nearly matches the observed variation in Fig. 7.

The rms differences between the estimated gravity and gravity from constant-density shape are shown in Fig. 9. It shows that the differences for the lower degrees are much larger than the gravity uncertainty (100 times for degree 2 and 10 times for degree 4). Differences are discernible to degree 6.

Polar Motion

The NEAR data allow an estimate of Eros' moments of intertia about the principal axes to be made and, as described earlier, the moments of inertia provide insight into the radial distribution of mass. Estimates of the moments of inertia cannot be obtained if Eros is in principal axis rotation and there is no free precession. Therefore, one of the priorities of the NEAR mission is to measure the free precession of Eros. Free precession is defined here as the Eulerian motion of the principal spin axis direction in the absence of external torques. Forced precession results from disturbances of Eros' rotational motion from quakes, impacts, or gravitational torques. The free precession resulting from distinct events will damp out depending on the rate of internal energy dissipation whereas the forced precession from external gravity sources persists but is low in amplitude. The Sun's gravity gradient produces a small forced precession and nutation and an even smaller free precession that is required for the angular momentum vector to change direction in inertial space.

The response of Eros to the solar gravity gradient torque depends on the orbit of Eros, the attitude and body-fixed spin vector of Eros at some reference epoch, and the intertia tensor. All of these parameters may be solved for with high precision except the diagonal elements of the intertia tensor and the components of spin in body-fixed coordinates normal to the angular momentum vector. The second-degree gravity harmonic coefficients provide the differences in the values of the diagonal elements of the inertia tensor, but the trace or any one diagonal element is needed to complete the inertia tensor. The complete intertia tensor may be obtained by numerical integration of the shape model. To minimize the error, only the smallest diagonal element is needed to complete the gravity-harmonic-based inertia tensor. Thus, the I_{xx} term of the shape model inertia tensor is used to augment the gravity-based inertia tensor.

The determination of the spin vector components normal to the angular momentum vector is needed to completely determine the free precession of Eros. These spin vector components place the angular momentum vector in Eros body-fixed coordinates. The normal spin vector components are too small to be resolved; however, the magnitude of the spin vector can be determined with very high precision. This high-precision measurement is obtained by observing, for several weeks, small craters near the ends of Eros whose motions can be observed at the 1-m level. The motion of the principal z axis projected onto the sky is shown in Fig. 10 as a function of right ascension and declination. The amplitude of the free precession is about 36 milliarcseconds and the forced precession over 3 days moves the pole and angular momentum vector about 1 arcsecond. This motion is too small to detect by the orbit determination filter. Figure 11 shows that the precession is about 0.01° over 9 years, which is well beyond the lifetime of the NEAR mission. However, the short-period nutation has an amplitude of 0.02° over 6 months and this can be detected. The solution obtained by processing 6 weeks of navigation data does not indicate free precession above that induced by the Sun's gravity. However, this does not rule out free precession from other sources with amplitudes up to as much as 0.01°.

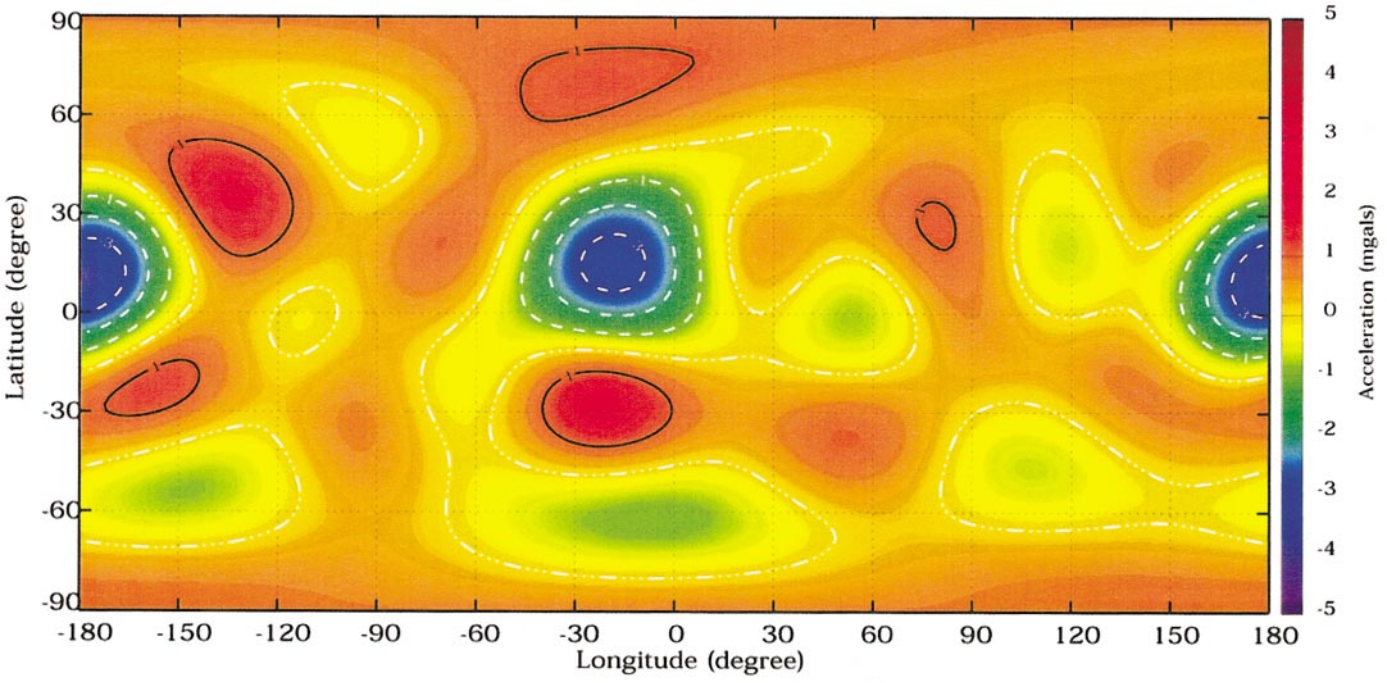

FIG. 7. The Eros Bouguer map. This displays the difference in acceleration on a 16-km sphere between the estimated gravity field and the gravity determined from a constant density shape model. The acceleration minimum is 3.86 mgal. Coefficients from degree 2 to degree 6 are included.

Particle Dynamics

Assuming a constant density for the asteroid, the polyhedron shape model of Eros can be used to compute the gravity field at the surface of the asteroid (Werner and Scheeres 1997). Spherical harmonic expansions are no longer valid in this regime and diverge due to the large ellipticity of the asteroid's shape.

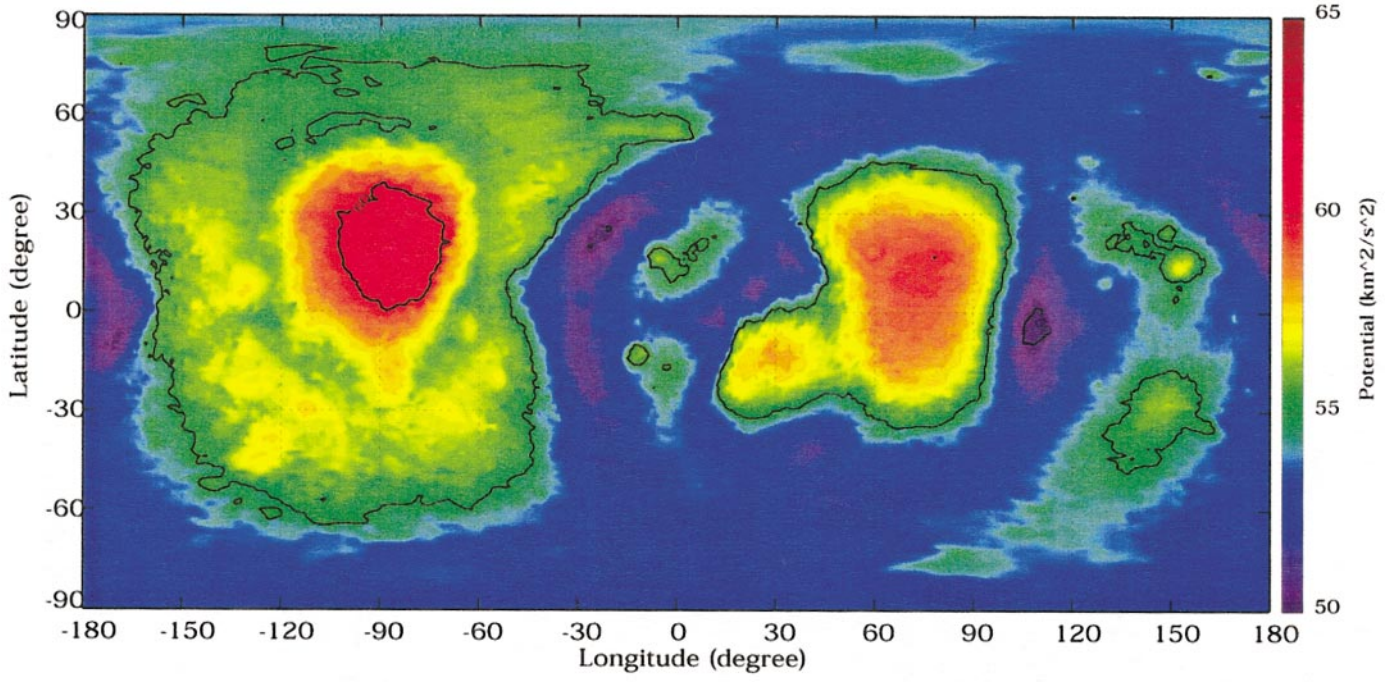

FIG. 8. The values of the gravitational plus rotational potential on the surface of Eros. The gravity potential is determined from a 56,644 polyhedra model of the Eros shape assuming constant density.

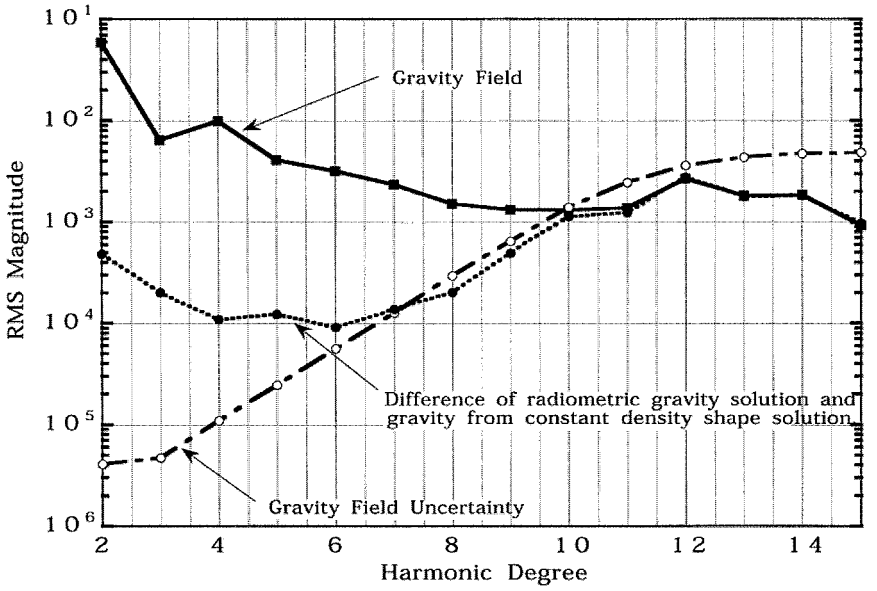

FIG. 9. The rms magnitude of the difference between the estimated gravity solution and the gravity determined from the constant density shape model.

Using the constant-density assumption in conjunction with the measured shape model, rotation pole, and rotation rate, a number of quantities of interest for the dynamical characterization of the asteroid can be computed (Scheeres *et al*. 1998). Over the entire surface of the asteroid we find that the slope (the angle between a plumb line and the local surface normal) ranges up to 49° with the average slope over the surface being 11.5°. In terms of slope distribution, only 1.5% of the surface area has a slope greater than 30°, indicating a relaxed surface. Surface normal accelerations on the asteroid vary from a minimum of 2.3 mm/s^2 to a maximum of 5.6 mm/s^2, and tangential accelerations range up to 3.7 mm/s^2. The speed sufficient to launch a surface particle directly onto an escape trajectory from Eros (when launched from the surface in the local normal direction) varies from 3.3 m/s to 17.3 m/s. The wide range in escape speeds and surface accelerations is due to variations in Eros' gravity and shape coupled with centripetal accelerations due to the asteroid's rotation.

The Roche lobe of the asteriod can also be computed using the measured models (Dobrovolskis and Burns 1980), in this case defined with respect to rotational forces rather than tidal forces (Scheeres *et al*. 1996). The Roche lobe is similar to an iso-energy surface that surrounds the asteroid and separates it from the rest of the Solar System. If a particle close to the asteroid has less than this energy, then it is impossible for it to "escape" from the asteroid. However, if a particle on the surface is given sufficient speed to increase its energy to the value of the Roche lobe (usually considerably less than escape speed as defined above) it becomes energetically possible for the particle to escape from the asteroid.

Note that a particle that is outside the Roche lobe will not fly off of the surface, as the local acceleration is still attractive in general. There are two ways in which to measure the distance of the asteroid surface from the Roche lobe: by computing the necessary speed for the particle energy to equal the lobe energy at each location on the asteroid surface or by computing the minimum distance the particle would have to be raised above the surface before it crosses the Roche lobe. This second computation includes the change in potential energy of a particle as it is lifted above the surface.

For the current Eros model the entire asteroid surface lies below the Roche lobe, although the distance between the asteroid surface and the Roche lobe is relatively small. The necessary speed for a surface particle to reach the Roche lobe energy ranges from 1 to 5 m/s over the asteroid surface and is always less than the local escape speed as defined earlier. Thus, it is possible for material to escape from the asteroid surface even if it initially has less than escape speed. The distance of the surface from the Roche lobe ranges from 0.09 to 2.67 km, with 56% of the surface lying within 1 km of the Roche lobe. Figure 12 shows the projection of the Roche lobe surface onto the Eros equatorial plane, with the Eros shape superimposed. The conformity between the surfaces extends over the entire three-dimensional shape. Eros is the first asteroid (discounting Phobos and Deimos) for which all data used in computing the Roche lobe have been directly measured to high accuracy.

The proximity of the asteroid surface to the Roche lobe seems to indicate that the asteroid surface is naturally constrained to lie within the lobe. The geological process that would result in this situation is currently unknown. It may be indicative of a regolith-covered asteroid. In this scenario, a regolith-covered region in close proximity to the Roche lobe could be easily excited by impact events and material might be given sufficient energy to escape from the asteroid, a dynamical process that

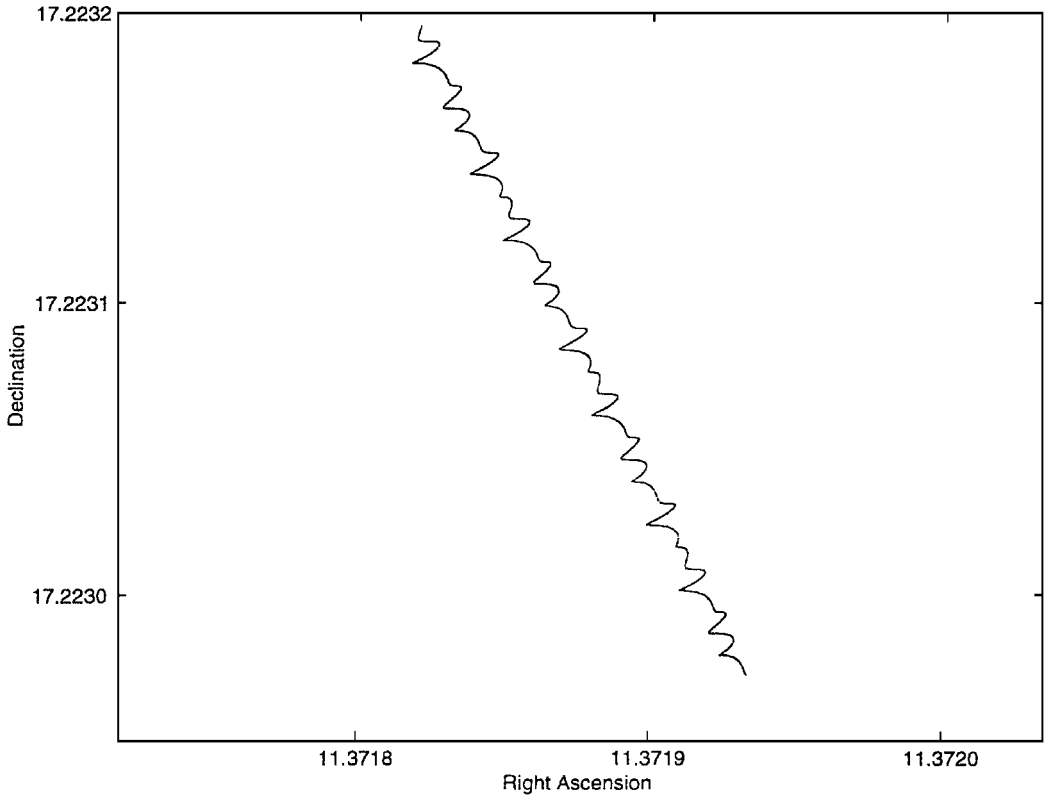

FIG. 10. Eros pole motion projected onto the sky. The short-period oscillation of Eros' pole, or free precession, is induced by the solar gravity gradient torque. If the solar torque was removed, the free precession of Eros would eventually damp out. Tick marks are at 60-day intervals.

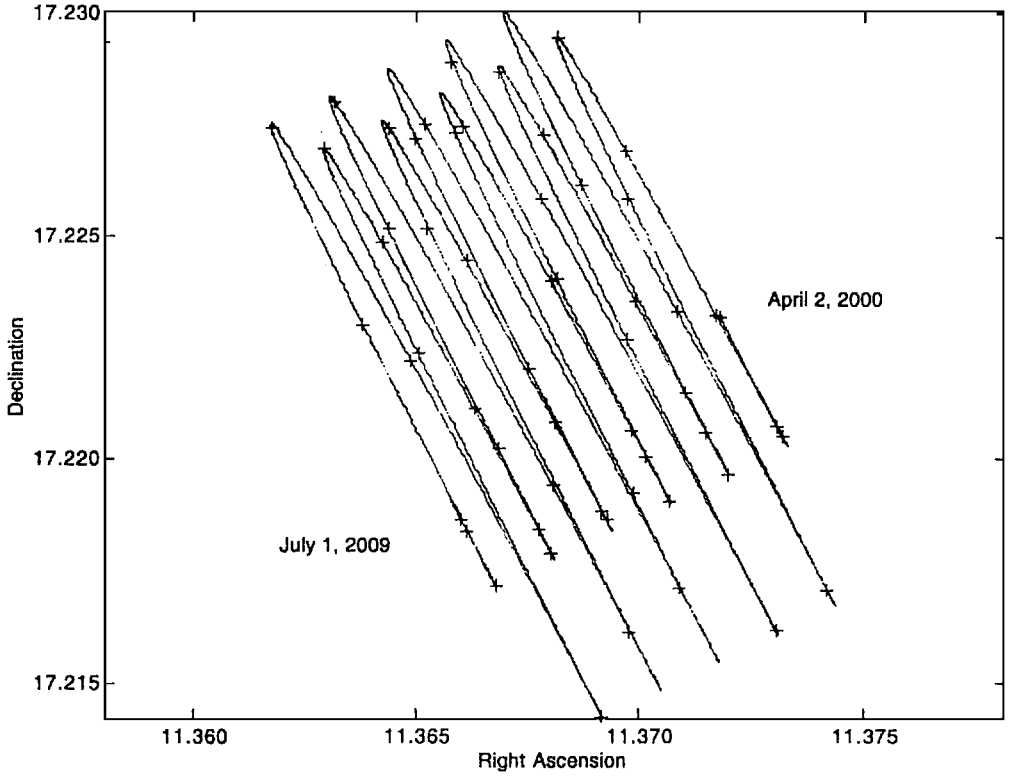

FIG. 11. The long-term motion of Eros' pole over 3 days (April 2, 2000 epoch). Shown are the forced precession and nutation caused by the solar gravity gradient mapped over several years.

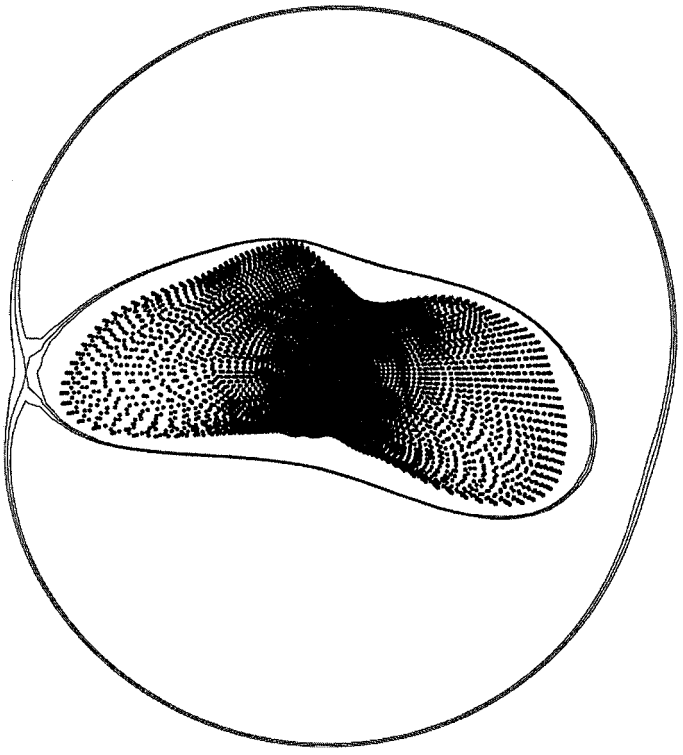

FIG. 12. Roche lobe projected onto the Eros equatorial plane, with the Eros shape superimposed. Note that neighboring values of energy are also plotted, showing the open Roche lobe and the closed Roche lobe.

would naturally constrain the asteroid to lie within its Roche lobe. It should be noted that any surface ejecta that escapes the Roche lobe may initially be in orbit about Eros but would eventually be ejected from the asteroid into a heliocentric orbit due to interactions between the orbiting particle and the Eros gravity field (Scheeres *et al*. 2000).

CONCLUSION

Our best estimates of the physical parameters describing Eros' shape, gravity field, spin state, and inertial properties have been presented. These estimates were determined as a necessary step in performing the precise navigation of the NEAR spacecraft in its orbit about asteroid 433 Eros. As such, the parameter values have been validated by the navigation accuracy of the NEAR trajectory. Because the utilized NEAR data sampled a wide range of attitudes and viewing geometry, we expect that only minor improvements in the physical parameter estimates could be obtained by processing tracking data for the remainder of the orbit phase. Gravity and shape results show the near uniformity of Eros to about the 1% level for the long-wavelength features. Variations in the gravity have been detected and may be explained in part by a regolith and/or internal density variations.

ACKNOWLEDGMENTS

The authors thank those who contributed to the success of NEAR navigation and radio science. The spacecraft design under the leadership of Tom Coughlin and Andy Santo, the mission design under the leadership of Bob Farquhar and David Dunham, and the mission operations under the leadership of Mark Holdridge, all employees of the Applied Physics Laboratory, were executed in a manner to ensure the success of navigation and radio science. The authors also are indebted to those who prepared data for processing by the orbit determination software. We thank Doug Holland (APL) of the NEAR Science Data Center for spacecraft attitude history and thrusting events files, Yanping Guo (APL) for preparing NLR data, and Scott Murchie (APL) and Mark Robinson (Northwestern University) for help in preparing MSI images. We are also indebted to Ann Harch, Maureen Bell, and Colin Peterson of Cornell University for planning MSI optical navigation images and Gene Heyler and Courtney Ray of APL for designing and operating the high-precision spacecraft attitude control system that made the optical navigation a success. The work described in this paper was carried out by the Jet Propulsion Laboratory, California Institute of Technology, under a contract with the National Aeronautics and Space Administration.

REFERENCES

Dobrovolskis, A. R., and J. A. Burns 1980. Life near the Roche limit: Behavior of ejecta from satellites close to planets. *Icarus* **42**, 422–441.

Dunham, D. W., R. W. Farquhar, J. V. McAdams, B. G. Williams, J. K. Miller, C. L. Helfrich, P. G. Antreasian, and W. M. Owen 1999. *Recovery of NEAR's Mission to Eros*. International Astronautical Congress Paper IAF-99-Q.5.05. Amsterdam, The Netherlands.

Ellis, J. 1980. Large scale state estimation algorithms for DSN tracking station location determination. *J. Astronaut. Sci.* **28**, 15–30.

Farquhar, R. W. (Ed.) 1995. Special issue on the Near Earth Asteroid Rendezvous mission. *J. Astronaut. Sci.* **43**.

Garmier, R., and J. P. Barriot 2000. Ellipsoidal harmonic expansions of the gravitational potential: Theory and application. *Celest. Mech. Dynam. Astron.*, in press.

Hawkins, S. E., and 12 colleagues 1997. Multi-spectral imager on the Near Earth Asteroid Rendezvous mission. *Space Sci. Rev.* **82**, 31–100.

Heiskanen, W. A., and H. Moritz 1967. *Physical Geodesy.* W. H. Freeman and Company, San Francisco.

Kaula, W. M. 1966. *Theory of Satellite Geodesy.* Blaisdell, Waltham, MA.

Konopliv, A. S., W. B. Banerdt, and W. L. Sjogren 1999. Venus gravity: 180th degree and order model. *Icarus* **139**, 3–18.

Miller, J. K., C. J. Weeks, and L. J. Wood 1990. Orbit determination strategy and accuracy for a comet rendezvous mission. *J. Guidance Control Dyn.* **13**, 775–784.

Miller, J. K., P. G. Antreasian, R. W. Gaskell, J. Giorgini, C. E. Helfrich, W. M. Owen, B. G. Williams, and D. K. Yeomans 1999. Determination of Eros physical parameters for Near Earth Asteroid Rendezvous orbit phase navigation. AAS Paper 99–463, presented at AAS/AIAA Astrodynamics Specialist Conference, Girdwood, Alaska.

Miller, J. K., P. G. Antreasian, J. J. Bordi, S. Chesley, C. E. Helfrich, A. Konopoliv, W. M. Owen, T. C. Wang, B. G. Williams, and D. K. Yeomans 2000. Determination of Eros' physical parameters from Near Earth Asteroid Rendezvous orbit phase navigation data. AIAA Paper 2000–4422, presented at AAS/AIAA Astrodynamics Specialist Conference, Denver, Colorado.

Moyer, T. D. 1971. *Mathematical Formulation of the Double-Precision Orbit Determination Program (DPODP).* JPL Technical Report 32-1527. Jet Propulsion Laboratory, California Institute of Technology, Pasadena, CA.

Scheeres, D. J., S. J. Ostro, R. S. Hudson, and R. A. Werner 1996. Orbits close to Asteroid 4769 Castalia. *Icarus* **121**, 67–87.

Scheeres, D. J., S. J. Ostro, R. S. Hudson, E. M. DeJong, and S. Suzuki 1998. Dynamics of orbits close to Asteroid 4179 Toutatis. *Icarus* **132**, 53–79.

Scheeres, D. J., B. G. Williams, and J. K. Miller 2000. Evaluation of the dynamic environment of an asteroid: Applications to 433 Eros. *J. Guidance Control, Dyn.* **23**(3), 466–475.

Thomas, P. C., and 18 colleagues 2002. Eros: Shape, topography, and slope processes. *Icarus* **155**, 18–37.

Veverka, J., and 25 colleagues 1999. Imaging of Asteroid 433 Eros during NEAR'S flyby reconnaissance. *Science* **285**, 562–564.

Veverka, J., and 33 colleagues 2000. NEAR at Eros: Imaging and spectral results. *Science* **289**, 2088–2097.

Werner, R. A., and D. J. Scheeres 1997. Exterior gravitation of a polyhedron. *Celest. Mech. Dynam. Astron.* **65**, 313–344.

Yeomans, D. K. 1995. Asteroid 433 Eros: The target body of the NEAR mission. *J. Astronaut. Sci.* **43**, 417–426.

Yeomans, D. K., P. G. Antreasian, A. Cheng, D. W. Dunham, R. W. Farquhar, R. W. Gaskell, J. D. Giorgini, C. E. Helfrich, A. S. Konopliv, J. V. McAdams, J. K. Miller, W. M. Owen Jr., P. C. Thomas, J. Veverka, and B. G. Williams 1999. Estimating the mass of Asteroid 433 Eros during the NEAR spacecraft flyby. *Science* **285**, 560–561.

Yeomans, D. K., P. G. Antreasian, J. P. Barriot, S. R. Chesley, D. W. Dunham, R. W. Farquhar, J. D. Giorgini, C. E. Helfrich, A. S. Konopliv, J. V. McAdams, J. K. Miller, W. M. Owen Jr., D. J. Scheeres, P. C. Thomas, J. Veverka, and B. G. Williams 2000. Radio science results during the NEAR-Shoemaker spacecraft rendezvous with Eros. *Science* **289**, 2085–2088.

Zuber, M. T., D. E. Smith, A. F. Cheng, J. B. Garvin, O. Aharonson, T. D. Cole, P. J. Dunn, Y. Guo, F. G. Lemoine, G. A. Neumann, D. D. Rowlands, and M. H. Torrence 2000. The shape of 433 Eros from the NEAR-Shoemaker laser rangefinder. *Science* **289**, 2097–2101.